Acta Crystallographica Section A
Foundations of Crystallography
ISSN 0108-7673

Received 14 September 2001
Accepted 22 October 2001

Excited-state structure by time-resolved X-ray diffraction

Christopher D. Kim,[a] Sebastien Pillet,[a] Guang Wu,[b] Wilfred K. Fullagar[b] and Philip Coppens[a]*

[a]Department of Chemistry, State University of New York at Buffalo, Buffalo, NY 14260-3000, USA, and [b]SUNY X3 Beamline, National Synchrotron Light Source, Brookhaven National Laboratory, Upton, NY 11973, USA. Correspondence e-mail: coppens@acsu.buffalo.edu

X-ray crystallography has traditionally been limited to the study of the ground-state structure of molecules and solids. Recent technical advances are removing this limitation as demonstrated here by a time-resolved stroboscopic study of the photo-induced 50 μs lifetime excited triplet state of the $[Pt_2(pop)_4]^{4-}$ ion [pop = pyrophosphate, $(H_2P_2O_5)^{2-}$], performed at helium temperatures with synchrotron radiation. The shortening of the Pt—Pt bond by 0.28 (9) Å upon excitation is compatible with the proposed mechanism involving promotion of a Pt—Pt antibonding $d\sigma^*$ electron to a weakly bonding p orbital. The contraction is accompanied by a 3° molecular rotation. The time-resolved diffraction technique described here is applicable to reversible light-driven processes in the crystalline solid state.

1. Introduction

Conventional X-ray crystallography has been traditionally limited to the study of the ground-state structure of molecules and solids. This limitation is now being removed as demonstrated by the rapid development of time-resolved biochemical crystallography, summarized in a recent review article (Moffat, 2001), and by a picosecond diffraction study of torsional distortions in the organic molecule *N*,*N*-dimethylaminobenzonitrile (DMABN) (Techert *et al.*, 2001). A parallel development of the EXAFS technique has recently been applied in the first time-resolved determination of the changes in coordination geometry in a transition-metal complex (Chen *et al.*, 2001). Macromolecular studies make use of the polychromatic Laue technique. They have been used to study processes such as CO dissociation from myoglobin (Srajer *et al.*, 1996; Moffat, 2001), and enzyme–substrate reactions, such as occur in isocitrate dehydrogenase (Stoddard *et al.*, 1998), and have been reviewed by Ren *et al.* (1999). We describe here the first application of monochromatic single-crystal methods to obtain information on a transient molecular excited state. A stroboscopic technique is used, in which the molecule is repeatedly excited, and the structural change probed for a period of microseconds, immediately after each of the more than 5000 excitations per second. The results indicate the feasibility of the approach, and point the way for the further refinement of the methods employed.

2. The excited state of the $[Pt_2(pop)_4]^{4-}$ ion

The distortion of the $[Pt_2(pop)_4]^{4-}$ ion [pop = pyrophosphate, $(H_2P_2O_5)^{2-}$] upon excitation to its lowest $^3A_{2u}(d\sigma^* \rightarrow p\sigma)$ triplet state has been previously investigated by spectroscopic techniques (Rice & Gray, 1983; Stiegman *et al.*, 1987) and by EXAFS (Thiel *et al.*, 1993). The excited state is split into ^3E_u and $^3A_{1u}$ levels, with a spacing of only 42 cm^{-1} (Fig. 1). As the lower $^3A_{1u}$ level has a much longer lifetime than the upper ^3E_u level (Markert *et al.*, 1983), the lifetime is strongly temperature dependent in the temperature region in which the 42 cm^{-1} splitting is larger than kT. As the Boltzmann constant $k = 0.7$ cm^{-1}, phosphorescence lifetime of $[Pt_2(pop)_4]^{4-}$ can be used as a probe of the sample temperature in the region below 40 K (Ribaud *et al.*, 2001).

3. Experimental

Time-resolved diffraction measurements were performed at the X3 beamline at the National Synchrotron Light Source, using instrumentation specifically designed for time-resolved stroboscopic pump-probe experiments (Fullagar *et al.*, 2000).

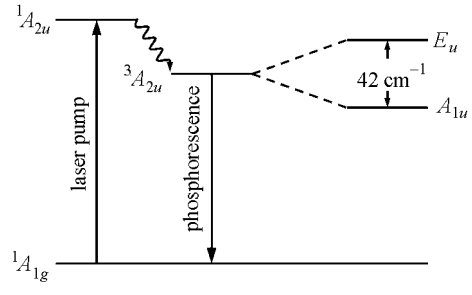

Figure 1
Schematic energy-level diagram of the Ptpop ion.

X-ray pulses are produced by inserting a rotating chopper wheel in the X-ray beam ($\lambda = 0.643$ Å). The number and width of the slots in the chopper wheel and the number of revolutions per second (rev s^{-1}) are selected to give a pulse width and frequency appropriate for the lifetime of the sample under investigation. In the current experiment, the frequency and X-ray pulse width were 5100 Hz and 33 μs, respectively, with an X-ray duty cycle of 17%. During the experiment, pulses from a tripled Nd/YAG pump laser (λ = 355 nm) are synchronized with the X-ray pulses. The light from the laser is guided through a tapered optical fiber and focused on a sample of 50 μm linear dimension. At the frequency of 5100 Hz, the energy per pulse focused on the crystal is in the 80–130 μJ range. In all experiments, the sample temperature was maintained at 17 K using a helium gas-flow system (Hardie *et al.*, 1998; Ribaud *et al.*, 2001). However, a small temperature increase occurs during irradiation, as described below. The phosphorescence of the sample was continuously observed during data collection, thus allowing temperature monitoring and detection of deterioration of the spectroscopic properties, which may not be evident in the diffraction pattern. The time structure of the experiment is depicted in Fig. 2.

The TEA (TEA = tetraethylammonium) salt has the composition $(TEA)_3H(Ptpop)$. This salt was selected rather than the potassium salt $K_4(Ptpop)$ because of its much better endurance of prolonged exposure to powerful laser pulses and the dilution of the active species by the bulky counterion, which has important advantages in time-resolved studies.

In the first stage of the experiment, the 17 K dark structure was recorded to provide a reference structure. The salt crystallizes in a monoclinic cell with half a $[Pt_2(pop)_4]^{4-}$ ion in the asymmetric unit of the space group $C2/c$, the two Pt atoms being related by a center of symmetry.[1] The acid proton is located in a short interionic hydrogen bond [2.469 (3) Å] connecting two center-of-symmetry-related terminal oxygen atoms and is distributed over two positions on each side of the center. The strong hydrogen bonds link the anions into a chain parallel to the *b* direction. One of the independent cations is in a general position, while the second, located on a twofold axis, exhibits a small orientational disorder, which could be refined from the He temperature data. An *ORTEP* diagram of the Ptpop ion is shown in Fig. 3.

In the second stage, light-on data collection during a 0.3° rotation (15 s duration, corresponding to 15 × 5100 laser-light pulses) of the sample alternated with light-off measurement over the same 0.3° rotation range. The minimization of the time delay between the on and off measurements provides essentially identical conditions during light-on and light-off data collection, and significantly increases the sensitivity of the experiment. Four light-on/light-off data sets, each covering a rotation range of 36°, were collected, corresponding to a total of 8876 reflections. After averaging over multiply-measured and symmetry-equivalent sets, 3513 unique intensities were obtained (R_{int} = 6.6 and 7.1% for the off and on data, respectively). The cell dimensions of the dark and light-on structures, as determined from the limited data sets, are identical within two standard deviations. While the standard deviations are relatively large, the differences between the on and off sets are within 0.1%, as may be expected given the small conversion percentage.

4. Analysis of the results

In the initial analysis of the light-induced intensity changes, a modified Wilson plot of $\ln(I_{on}/I_{off})$ *versus* $(\sin\theta/\lambda)^2$, where I_{on} and I_{off} are the measured intensities during the light-on and light-off periods, respectively, and θ is the Bragg angle of the reflection, was constructed for each of the four sets. The plot for the first set is shown in Fig. 4. In the low-order region, both intensity increases and decreases are observed upon light exposure. With increasing $(\sin\theta/\lambda)^2$, the intensity decreases, the slope being $2\Delta B = 0.43$ Å^2 for the plot shown, indicating an increase in the overall isotropic atomic displacement parameter (ADP). The increase varies among the four sets, a variation attributed to slight differences in the position of the crystal in the narrow liquid-helium stream. The average increase in the overall atomic displacement parameter is

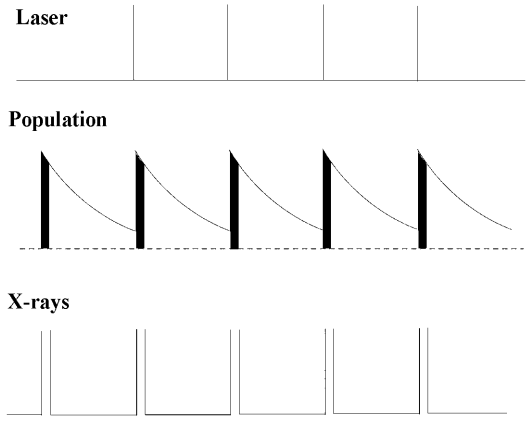

Figure 2
The time structure of the stroboscopic X-ray experiment. For the experimental frequency of 5100 Hz, the spacing between adjacent maxima is 196 μs. The width of the X-ray pulse in the current experiment is 33 μs.

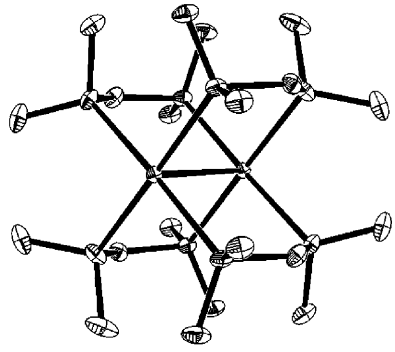

Figure 3
ORTEP diagram of the PtPop ion at 17 K. 50% probability ellipsoids.

[1] Cell dimensions: $a = 22.2118$, $b = 10.1990$, $c = 21.5975$ Å, $\beta = 112.501°$ at 17 K.

Table 1
Comparison of ΔB values for the four experimental runs.

Set	ΔB from Wilson-type plot (Å^2)	Temp. scale factor, k_B	ΔB from k_B (based on $B_{\rm dark}$ = 0.79 Å^2)
1	0.215 (10)	1.266 (4)	0.210
2	0.175 (5)	1.210 (3)	0.166
3	0.395 (10)	1.432 (4)	0.341
4	0.255 (10)	1.304 (3)	0.240

0.26 Å^2, which may be compared to the equivalent isotropic ADP of the dominantly scattering Pt atom of 0.79 Å^2 in the dark structure. Part of the increase is due to the presence of a second species generated by the excitation, as further discussed below.

Least-squares refinements of each of the four subdata sets with a temperature scale factor defined by

$$B_{\rm light\ on} = k_B B_{\rm light\ off} \qquad (1)$$

(Ozawa *et al.*, 1998) closely reproduce the results from the Wilson plots, as summarized in Table 1.

The light-induced structural change can be illustrated by a *photodifference* map (Carducci *et al.*, 1997), which shows the change in electron density upon light exposure and is obtained by Fourier summation with coefficients equal to the difference between the 'on' and 'off' structure factors. To construct the photodifference map, the four data sets were brought on a common temperature scale using the ΔB values from the Wilson plot, on a proper relative scale with the *Scalepack* programs (Otwinowski & Minor, 1997) and on an absolute scale by refinement of the conventional scale factors against the basic structure. The resulting photodifference map (Fig. 5) gives clear evidence for a displacement of the Pt atoms in a direction towards the other Pt atom in the molecular ion. The direction of the displacement does not coincide exactly with the intramolecular Pt—Pt vector, indicating that a small molecular rotation accompanies the shortening of the Pt—Pt bond on excitation.

Subsequent quantitative analysis of the changes is based on least-squares refinement of the response ratios, defined as

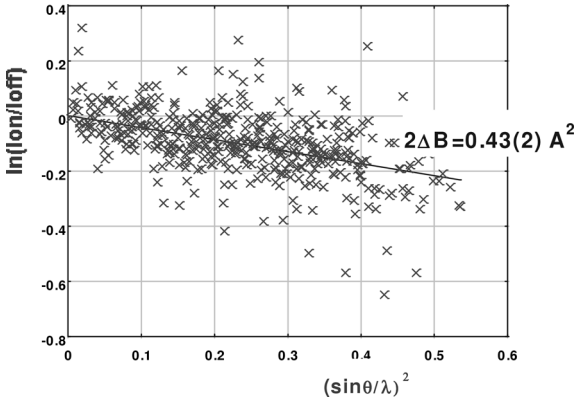

Figure 4
Modified Wilson plot showing the relation between I(light-on) and I(dark) as a function of $(\sin\theta/\lambda)^2$.

Table 2
Agreement factors on η for different sets of reflections.

	$\eta/\sigma > 0$	$\eta/\sigma > 1$	$\eta/\sigma > 2$	$\eta/\sigma > 3$
Number of η values	3513	2358	1500	968
$\langle\eta/\sigma\rangle$	2.28	3.16	4.13	5.04
$R(\eta)$†	0.50	0.34	0.29	0.26

† Defined as $\sum(\eta_{\rm obs}-\eta_{\rm calc})/\sum\eta_{\rm obs}$.

$$\eta = (I_{\rm on} - I_{\rm off})/I_{\rm off} \qquad (2)$$

(Coppens, 1992; Ozawa *et al.*, 1998). Statistics of η given in Table 2 show that the measured changes are statistically significant. The refinement uses the information from the stage 1 dark structure determination, while varying the x, y and z coordinates of the Pt atom of the light-induced triplet state and the temperature scale factors for each of the four data sets collected in the stage 2 experiments. While all reflections were included, the results were not affected by the use of different η/σ cut-offs. The refinement was repeated for different values of the excited-state population. The lowest value of $R(\eta)$ is obtained for a population of 2.0%, with an uncertainty estimated from the change in R and the Pt—Pt bond-length standard deviation of about 0.3%. The small conversion percentage leads to a large standard deviation in the coordinates of the excited-state Pt atom.

Results are summarized in Tables 2 and 3, which list η-based agreement factors, $\langle\eta/\sigma\rangle$ values, Pt coordinates and the Pt—Pt bond lengths in the ground and triplet states.

The significant shortening of the Pt—Pt bond by 0.28 (9) Å is as expected from the proposed mechanism of the excitation, in which a Pt—Pt antibonding $d\sigma^*$ electron migrates to a weakly bonding p orbital. The reduction in size of the mole-

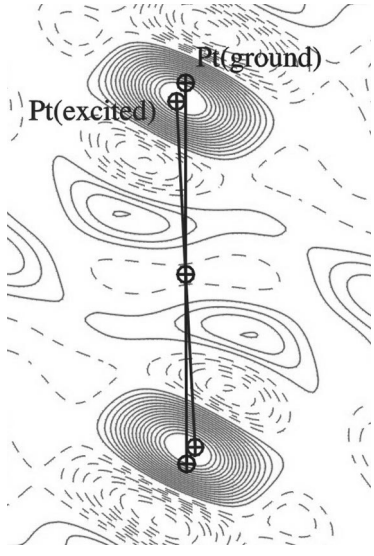

Figure 5
Photodifference map in the plane of the Pt—Pt bond bisecting two Pt—P vectors. A center of symmetry is located at the circle in the center of the drawing. Continuous lines positive, dashed lines negative. Contours at 0.1 e Å^{-3}.

cule is accompanied by a slight rotation of ~3°, in accordance with the location of the peaks in the photodifference map.

5. Discussion

5.1. The temperature increase

The increase in the atomic displacement parameter (ADP) is in part due to the creation of a second, excited-state species in the crystal and in part due to a temperature increase during the light-exposure period. Based on the excited-state population and the Pt displacement obtained from the least-squares refinement, the 'disorder contribution' to the increase in the mean-square displacement is about 0.12 Å^2. The remaining contribution ranges from 7 to 35% of the ADP of the dominantly scattering Pt atom for the different data sets. The corresponding temperature increase depends on the relative contribution of the different modes in the crystal, only the softest of which will not be reduced to their zero-point vibrations at the experimental temperature of 17 K. If we assume that the mean-square displacements are proportional to T, but with a proportionality factor of 0.5 rather than 1 as is the case in the classical region, the average temperature increase would be about 6°.

5.2. The contraction of the Pt—Pt bond

The results may be compared with those obtained in previous spectroscopic studies. From the Franck–Condon analysis of the vibrational fine structure of the absorption and emission spectra, a shortening of 0.21 Å was deduced (with an error estimated at 10–15%), but using the assumption that the metal–metal stretch only involves the Pt atoms (Rice & Gray, 1983). This corresponds to a Pt—Pt excited-state bond length of 2.71 Å. A second study, based on Raman data and using the empirical Badger's rule, which relates a change in stretching frequency with a change in bond length, leads to a value of 2.81 Å (Stein *et al.*, 1983). EXAFS results have been used to derive a contraction of 0.52 (13) Å of the P planes along the Pt—Pt axis but are based on an assumed Pt—Pt excited-state distance of 2.75 Å (Thiel *et al.*, 1993). Theoretical DFT (density functional theory) calculations of the excited-state structure, to be published elsewhere (Novozhilova & Coppens, 2001), confirm the shortening of the Pt—Pt bond, though the theoretical value is quite dependent on the functionals used in the calculation.

6. Concluding remarks

The current result is the first direct measurement of an interatomic distance in a molecule in its excited triplet state. The time-resolved stroboscopic diffraction method employed is not limited to the determination of the change in a single distance as in the current experiment, in which the scattering of the Pt atoms dominates the diffraction. Much faster measurements now being planned at the third-generation Advanced Photon Source will allow collection of more extensive data sets and the use of smaller crystals, which should make it possible to reach larger excited-state concentrations, and thus offer an increase in the sensitivity and accuracy of the method. The stroboscopic time-resolved diffraction method is applicable to reversible light-driven processes in the crystalline state, including solids in which photoactive molecules are embedded in three-dimensionally ordered supramolecular crystals (Zhang *et al.*, 2000; Ma *et al.*, 2001). As the method can be applied to many systems, among which are molecules and molecular assemblies involved in photosynthetic reactions, vision and energy storage, further applications providing insight into a wide range of dynamic processes may be anticipated.

Table 3
Pt positional parameters and Pt—Pt bond lengths.

	x	y	z	Pt—Pt bond length (Å)
Ground state	0.758392 (4)	0.165212 (7)	0.556967 (4)	2.9126 (2)
Excited state	0.756 (2)	0.168 (5)	0.549 (2)	2.63 (9)

We thank the National Science Foundation (CHE9981864), the US Department of Energy (DE-FG02-86ER45231 and the Petroleum Research Fund of the American Chemical Society (PRF32638AC3) for financial support of this work. Research carried out in part at the National Synchrotron Light Source at Brookhaven National Laboratory, which is supported by the US Department of Energy, Division of Materials Sciences and Division of Chemical Sciences. We thank Gary Sagerman and Lynn Ribaud for expert assistance in the construction of the instrumentation and operation of the facility. The Ar ion laser used in the experiment was provided under NSF grant no. CHE0087817 to Chem/Mat CARS at the Advanced Photon Source.

References

Carducci, M. D., Pressprich, M. R. & Coppens, P. (1997). *J. Am. Chem. Soc.* **119**, 2669–2678.
Chen, L. X., Jäger, W. J. H., Jennings, G., Gosztola, D. J., Munkholm, A. & Hessler, J. P. (2001). *Science* **292**, 262–264.
Coppens, P. (1992). *Synchrotron Radiation Crystallography*. London: Academic Press.
Fullagar, W. K., Wu, G., Kim, C. D., Ribaud, L., Sagerman, G. & Coppens, P. (2000). *J. Synchrotron Rad.* **7**, 229–235.
Hardie, M. J., Kirschbaum, K., Martin, A. & Pinkerton, A. A. (1998). *J. Appl Cryst.* **31**, 815–817.
Ma, B.-Q., Zhang, Y. & Coppens, P. (2001). *Cryst. Eng. Commun.* **20**, 1–3.
Markert, J. T., Clements, D. P. & Corson, M. R. (1983). *Chem. Phys. Lett.* **97**, 175–179.
Moffat, K. (2001). *Chem. Rev.* **101**, 1569–1582.
Novozhilova, I. & Coppens, P. (2001). To be published.
Otwinowski, Z & Minor, W. (1997). *Methods Enzymol.* **276**, 307–326.
Ozawa, Y., Pressprich, M. R. & Coppens, P. (1998). *J. Appl. Cryst.* **31**, 128–135.
Ren, Z., Bourgeois, D., Helliwell, J. R., Moffat, K., Srajer, V. & Stoddard, B. L. (1999). *J. Synchrotron Rad.* **6**, 891–917.
Ribaud, L., Wu, G., Zhang, Y. & Coppens, P. (2001). *J. Appl. Cryst.* **34**, 76–79.

Rice, S. F. & Gray, H. B. (1983). *J. Am. Chem. Soc.* **105**, 4571–4575.
Srajer, V., Teng, T.-Y., Ursby, T., Pradervand, C., Ren, Z., Adachi, S., Schildkamp, W., Bourgeois, D., Wulff, M. & Moffat, K. (1996). *Science*, **274**, 1726–1729.
Stein, P., Dickson, M. K. & Roundhill, D. M. (1983). *J. Am. Chem. Soc.* **105**, 3489–3494.
Stiegman, A. E., Rice, S. F., Gray, H. B. & Miskowski, V. M. (1987). *Inorg. Chem.* **26**, 1112–1116.
Stoddard, B. L., Cohen, B. E., Brubaker, M., Mesecar, A. D. & Koshland, D. E. Jr (1998). *Nature Struct. Biol.* **5**, 891–897.
Techert, S., Schotte, F. & Wulff, M. (2001). *Phys. Rev. Lett.* **86**, 2030–2033.
Thiel, D. J., Lîviņš, P., Stern, E. A. & Lewis, A. (1993). *Nature (London)*, **362**, 40–43.
Zhang, Y., Kim, C. D. & Coppens, P. (2000). *Chem. Commun.* pp. 2299–2300.